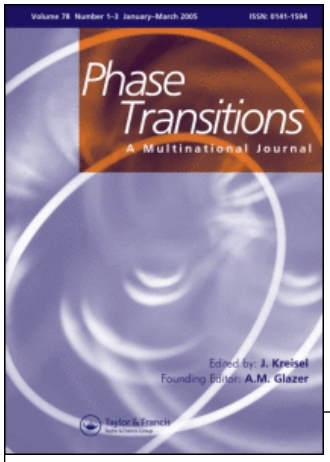

Phase Transitions
A Multinational Journal
Publication details, including instructions for authors and subscription information:
http://www.informaworld.com/smpp/title~content=t713647403

Shape recovery mechanism observed in single crystals of Cu-Al-Ni shape memory alloy

H. Seiner [ab]; P. Sedlák [ab]; M. Landa [a]
[a] Institute of Thermomechanics ASCR, 182 00 Prague 8, Czech Republic
[b] Faculty of Nuclear Sciences and Physical Engineering, CTU in Prague, 120 00 Prague 2, Czech Republic

First Published: June 2008

To cite this Article: Seiner, H., Sedlák, P. and Landa, M. (2008) 'Shape recovery mechanism observed in single crystals of Cu-Al-Ni shape memory alloy', Phase Transitions, 81:6, 537 — 551

To link to this article: DOI: 10.1080/01411590801891616
URL: http://dx.doi.org/10.1080/01411590801891616

Phase Transitions
Vol. 81, No. 6, June 2008, 537–551

Shape recovery mechanism observed in single crystals of Cu–Al–Ni shape memory alloy

H. Seiner[ab]*, P. Sedlák[ab] and M. Landa[a]

[a]*Institute of Thermomechanics ASCR, Doleškova 5, 182 00 Prague 8, Czech Republic;* [b]*Faculty of Nuclear Sciences and Physical Engineering, CTU in Prague, Trojanova 13, 120 00 Prague 2, Czech Republic*

(*Received 16 October 2007; final version received 3 January 2008*)

Micromechanism of the shape recovery process is optically observed in single crystals of the Cu–Al–Ni shape memory alloy. Formation of X and λ-interfaces (interfacial microstructures with two intersecting habit planes) is documented, both in a thermal gradient and during a homogeneous heating. The observed growth mechanisms (i.e. mechanisms of nucleation and growth of the twinned structures) are described and analysed. Weakly non-classical boundaries between austenite and two crossing twinning systems are also documented.

Keywords: shape memory alloys; shape recovery process; martensitic microstructure; non-classical boundaries

1. Introduction

The shape memory alloys (SMAs), exhibiting unique thermomechanic properties due to reversible martensitic transitions, have been thoroughly experimentally investigated since the discovery of the memory effect in 1950s. Especially the Cu–Al–Ni alloy which has been of enormous interest (see the list of experimental literature in [1] containing more than 80 items), as this alloy can be easily prepared, and slight changes in heat treatment enable the transition temperatures of this alloy to be adjusted for particular applications. However, only few works can be found on thermally induced transitions, particularly on the shape recovery process (the return from reoriented martensite to the parent austenitic phase), although this process plays a key role in the memory effect. In 1954, Basinski and Christian [2] used a thermal gradient to induce an austenite-to-martensite transition in the Indium–Thallium alloy and documented the microstructures they observed. In 1978, Salzbrenner and Cohen [3] investigated the thermally driven transitions in Cu–Al–Ni (both the austenite-to-martensite transition and the reverse transition from self-accommodated martensite into austenite). They observed a jerky character of propagation of the interface and recorded the temperature in four points at the surface of the specimen during the propagation. Similar experiments were repeated recently by Seiner et al. [4], who,

*Corresponding author. Email: hseiner@it.cas.cz

ISSN 0141–1594 print/ISSN 1029–0338 online

DOI: 10.1080/01411590801891616
http://www.informaworld.com

in addition, measured the dependence of propagation speed on the thermal gradient and described the observed *interfacial microstructure*, which means the microstructure forming between the austenite and martensite during the transition (more exact explanation of the term *interfacial microstructures* is given below). The moving interfacial microstructure observed by Seiner et al. between single variant of martensite and austenite was very similar to that described by Basinski and Christian. It consisted of two intersecting habit planes separating the austenite from twinned martensitic regions and two other intersecting planar boundaries between the twinned regions and the single variant of martensite. Basinski and Christian called this structure the *X*-interface or λ-interface depending on whether the twins inside the twinned regions were oriented parallel to the twinned-to-single variant boundaries or not. Ignácová et al. [5] observed a more complicated form of the λ-interfaces during the shape recovery of Cu–Al–Mn single crystals. Similar interfacial structures were also observed during stress-induced transitions, firstly by Sakamoto and Shimizu [6] and later by Shield [7].

In the both cases, the examined material was Cu–Al–Ni, however, although these microstructures had mesoscopic morphologies similar to the *X*-interfaces described in [2,4] and in this article, their microscopic structure is completely different.

In 1994, Ruddock [8] tried to explain the *X*-interface observed by Basinski and Christian by means of the mathematical theory of martensitic microstructures – a powerful theoretical tool introduced by Ball and James [9] and verified on numerous experimental results as summarized in the book by Bhattacharya [10]. Surprisingly, Ruddock proved that the *X*-interface (even if the twinned-to-single variant boundaries are allowed to be not exactly parallel to the twinning planes) cannot satisfy the compatibility conditions for In–Tl without elastic deformation, and thus, the material with such microstructure must be elastically deformed to achieve the compatibility. Ruddock concluded that, according to the theory of Ball and James, the *X*-interface cannot form spontaneously near the transition temperatures, and suggested less constrictive theories to be used for description of such interfacial microstructure. Ruddock also discussed similar incompatibility problem for the wedge microstructure, later analysed by Balandraud and Zanzotto [11], who quantified the difference of this microstructure from full compatibility and evaluated the accompanying elastic strain field. However, similar analysis for λ and *X*-interfaces is still missing.

This article brings a more detailed description of the microstructure observed in Cu–Al–Ni during the shape recovery process by Seiner et al. [4]. It aims to document that the *X* and λ-interfaces form spontaneously in the thermal gradients (i.e. they are not created artificially by forced crossing of two habit planes as it was done in [2]) and propagate stably even if the gradient is replaced by a homogeneous heating. These phenomena are observed in two specimens with different dimensions, crystallographic orientations and transition temperatures.

2. Shape recovery process in Cu–Al–Ni

We will use the term *shape recovery process* for a return of the martensitic lattice, either microstructured or a single variant, to the austenitic parent phase due to a temperature increase, whenever is this return accompanied by a change of the macroscopic shape of the specimen. Before we proceed to detailed discussion of this process, the following section is inserted to briefly recapitulate a basic theoretical background of martensitic transitions in SMAs.

2.1. *Habit planes and kinematic compatibility*

Both the austenite-to-martensite transition and the backward martensite-to-austenite transition are provided by motion of planar interfaces, so-called *habit planes*. The martensitic microstructure forming such coherent planar interface with austenite cannot be arbitrary, as the system is restricted by *kinematic compatibility condition* to be fulfilled at each habit plane. This condition reads

$$\mathbf{I} - \mathbf{M} = \boldsymbol{a} \otimes \boldsymbol{n}, \tag{1}$$

where $\mathbf{I}$ is a unit matrix representing here a deformation gradient of austenite (i.e. no deformation), $\mathbf{M}$ stands for the deformation gradient of the volume transformed into martensite, $\boldsymbol{n}$ is a unit vector normal to the habit plane and $\boldsymbol{a}$ is a *shearing vector*, which is the vector containing the information about magnitude and direction of the shearing mechanism accompanying the transition [10]. The existence of such shearing vector, i.e. the satisfaction of (1), is a necessary and sufficient condition for the existence of the $\mathbf{I} - \mathbf{M}$ compatible interface. In general, $\mathbf{M}$ can be either a single variant or a compatible (i.e. geometrically possible) mixture of variants with a homogeneous macroscopic deformation gradient.[1] Set of all such microstructures forms a quasiconvexification [12]

$$\{\mathbf{M} : \mathbb{R}^3 - \mathbb{R}^3 | \mathbf{M} \text{ compatible and } \mathbf{M} \text{ homogeneous}\} = \mathcal{Q}\left(\bigcup_{i=1}^{N} SO(3)\mathbf{U}_i\right). \tag{2}$$

Here, $\mathcal{Q}$ means a quasiconvex hull [13], $SO(3)$ is a group of all orthogonal rotations and $\mathbf{U}_i$ are *Bain tensors* of N possible martensitic variants. In our case of the Cu–Al–Ni alloy, which undergoes a cubic-to-orthorhombic transition, $N = 6$, i.e. all gradients $\mathbf{M}$ from this quasiconvexification can be constructed from six different variants of martensite. The simplest and most usually observed microstructures are the first-order laminates, which means that the microstructure consists of parallel laminas of two different variants. Let us denote these two variants by capital letters A and B, and let us assume that the variant B has a homogeneous volume fraction in the laminate and denote this volume fraction by λ. Then, the deformation gradient of the resulting microstructure is

$$\mathbf{M} = (1 - \lambda)\mathbf{R}_A\mathbf{U}_A + \lambda\mathbf{R}_B\mathbf{U}_B, \tag{3}$$

where $\mathbf{R}_{A,B} \in SO(3)$ are orthogonal rotations and $\mathbf{U}_{A,B}$ are Bain tensors of variants A and B, which form the laminar microstructure. The compatibility conditions inside the structure $\mathbf{M}$ must be satisfied as well, which adds a condition

$$\mathbf{R}_A\mathbf{U}_A - \mathbf{R}_B\mathbf{U}_B = \boldsymbol{b} \otimes \boldsymbol{m}, \tag{4}$$

where $\boldsymbol{m}$ is the unit vector normal to the laminas and $\boldsymbol{b}$ is, again, the shearing vector. The interface between two variants in the microstructure $\mathbf{M}$ is called the *twinning plane*. The interface between the first-order laminate and austenite is sometimes called a *classical boundary*. Habit planes and twinning systems able to form such type of boundary have been already determined for most of the commonly used materials, as can be found e.g. in [10]. In Cu–Al–Ni, three different twinning systems are possible. These are the Type-I twins, the Type-II twins and the Compound twins. However, as shown in [10], the Compound system is not able to form an interface with autenite, as it cannot fulfill the condition (1).

However, the condition (1) does not restrict the system to the classical boundaries. Any structure from quasiconvexification (2) satisfying this condition can form a planar

interface with austenite, moreover, the planarity of the interface can be also violated (see [12] for a speculative example.) Then, we speak about so-called *non-classical boundaries*, which have not been thoroughly investigated yet, neither on a theoretical level, nor experimentally.

2.2. *Mechanical stabilization of martensite*

Let us now consider a single crystal of austenite at sufficiently high temperature where the austenitic phase is stable, and let us subject this single crystal to a thermal procedure outlined in Figure 1(a). Under some critical temperature M_s, habit planes spontaneously form in the crystal, and it undergoes, by motion of these habit planes, a transition into martensite. Under the M_f temperature, the crystal is fully transformed into martensite. The transition is provided by propagation of the habit planes. For this reason, the resultant microstructure in martensite is able to satisfy the compatibility condition (1) over

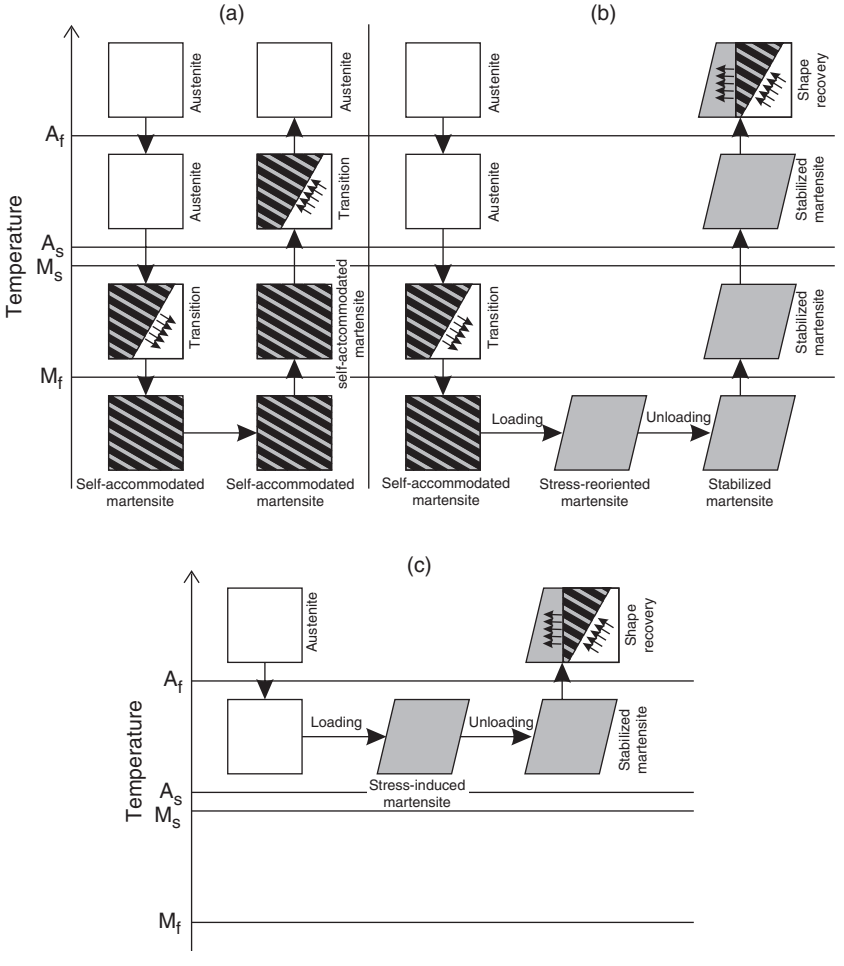

Figure 1. A purely thermal cycle applied to a single crystal of a shape memory alloy (a) compared to mechanical stabilization of martensite (b, c).

some of the possible habit planes. The resulting martensitic crystal has, macroscopically, the same shape as the parent austenitic crystal, which is usually called a *self-accommodation* of martensite. After heating such crystal back up again, a reverse transition occurs between temperatures A_s and A_f, and is provided by motion of habit planes backward through the compatible structures. The transition temperatures M_s, M_f, A_s and A_f are specific for each material and heat treatment, and can be obtained by DSC measurements.

The behaviour of such single crystal changes significantly after a mechanical loading (e.g. uniaxial compression) on the crystal is applied, as outlined in Figure 1(b, c). If the stress is applied at temperatures below M_f, the the self-accommodated martensite reorients into another microstructure (e.g. into a single variant). Such microstructure then stays stable after the loading is removed. When the specimen with such stress-reoriented microstructure is heated back, it cannot start transforming directly back to austenite at A_s, as this microstructure is not able to satisfy the compatibility condition (1), i.e. this microstructure does not allow the habit planes to move through the specimen. Thus, the transition front itself must be preceded by reorientation of the microstructure such that the compatibility is attained. This shifts the critical temperature for the martensite-to-austenite transition upwards, which is a phenomenon often called *mechanical stabilization of martensite*[2], and observed both in single crystals [14] and polycrystals [15]. In the following shape recovery process, the mechanical behaviour of the crystal (mechanics of the microstructure), and the driving thermal process (the phase transition itself) are thus, strongly coupled.

The mechanical stabilization of martensite can be also observed in stress-induced transitions. When an austenitic specimen at temperature higher then M_f (or even higher than A_f) is subjected to proper mechanical loading, it transforms into a stress-induced martensite. However, due to the mechanical stabilization and consequent shift in the critical temperature, this stress-induced martensite may stay stable after the loading vanishes, and requires further heating to transform back into austenite.

2.3. *Theoretical predictions for interfacial microstructures*

During the shape recovery process from the mechanically stabilized martensite, new microstructure in the crystal must form such that it enables compatible connection between austenite and the mechanically stabilized martensite. In the other words, the interfacial microstructure $\mathbf{M}$ must be able to satisfy the conditions (1) at the habit planes, simultaneously with similar conditions

$$\mathbf{S} - \mathbf{M} = \tilde{\boldsymbol{a}} \otimes \tilde{\boldsymbol{n}}, \tag{5}$$

at all planar interfaces between this microstructure and the mechanically stabilized martensite with deformation gradient $\mathbf{S}$. Here, $\tilde{\boldsymbol{n}}$ denotes the unit vector normal to such planar interface and $\tilde{\boldsymbol{a}}$ stands for the corresponding shearing vector. In the rest of the text, we will call this microstructure an *interfacial microstructure*, because it provides an interface between austenite and the mechanically stabilized martensite. Mobility of such microstructure is, then, a key point to dynamics of the whole transition.

Let us now discuss, what interfacial microstructures can be expected to appear. For simplicity, we will consider the mechanically stabilized martensite to be always a single variant (i.e. one variant of martensite without any twins) in our predictions. The simplest microstructure that can provide a compatible connection between austenite and single

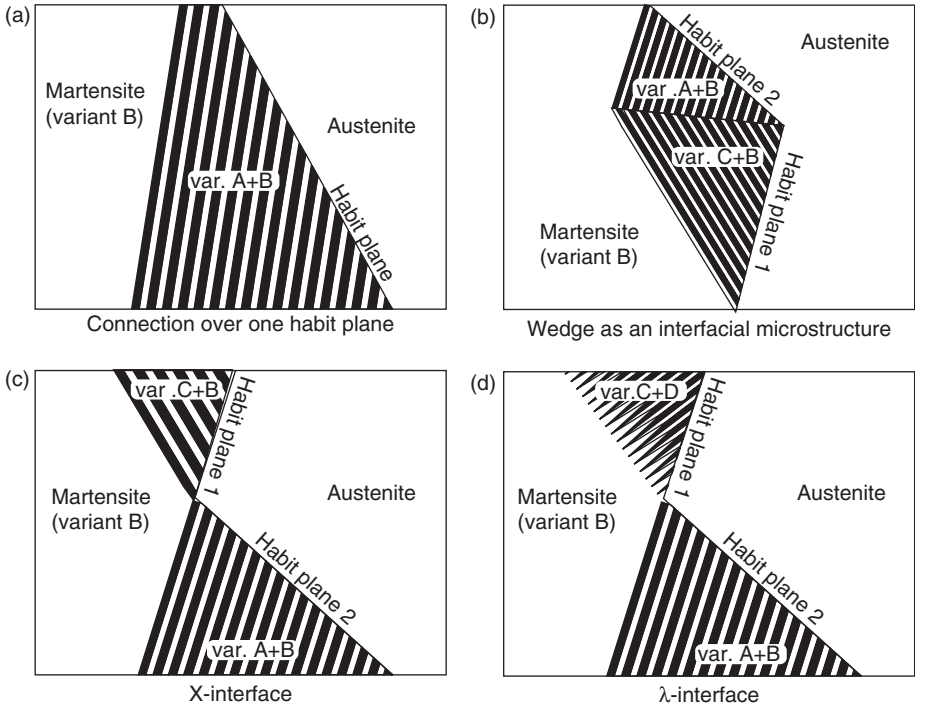

Figure 2. Possible interfacial structures between austenite and a single variant of martensite: (a) The connection over one habit plane, (b) The wedge microstructure as an interfacial microstructure, (c) The *X*-interface with twinned-to-single variant boundaries parallel to the twins, (d) The λ-interface.

variant of martensite is a homogeneously twinned region, which borders to austenite over one classical boundary. Such twinned region must be, compatibly again, connected to the mechanically stabilized martensite (Figure 2(a)). A more complicated family of interfacial structures can be obtained by considering two intersecting habit planes separating the austenite from the twinned regions.

In general, the intersection of two habit planes may lead to two principally different interfacial microstructures. If the habit planes are oriented such that the twinned regions behind them touch each other by a plane (Figure 2(b)), we obtain a so-called *wedge microstructure* [10,11]. Although a compatible connection of these touching twinned regions to single variant of martensite is theoretically possible, wedges as interfacial microstructures (i.e. wedges as microstructures providing compatible connections between austenite and stabilized martensite) are not mentioned in the available experimental literature yet. If the twinned regions behind the habit planes are fully separated from each other by the twinned-to-single variant planes, and touch each other, thus, only in one line, we obtain the *X*-interface or λ-interface (Figure 2(c, d)). For clarity, we will distinguish between these two microstructures using the same convention as Basinski and Christian [2], who used the term *X*-interface only for the case when the twinned-to-single variant boundaries were parallel (or nearly parallel) to the lamina inside the twinned regions. All other structures will be called λ-interfaces. In these two types of interfaces, the single variant of martensite coincides with the austenite always in one line inside the specimen.

Table 1. Transition temperatures, face orientations and dimensions of the examined Cu–Al–Ni specimens.

Faces	Orientation in austenite [unit face normal]	Dimensions in austenite [mm]	Orientation in martensite [unit face normal]	Dimensions in martensite [mm]
Specimen #1 DSC: $M_s = -35°C$, $M_f = -58°C$, $A_s = -6°C$, $A_f = 22°C$				
A, C	[0.98; −0.21; 0.02]	11.85×3.18	[0.53; 0.02; 0.85]	11.01×3.30
B, D	[0.20; 0.98; 0.00]	11.85×3.13	[0.83; 0.00; −0.56]	11.01×3.23
Specimen #2 DSC: $M_s = -5°C$, $M_f = -22°C$, $A_s = 26°C$, $A_f = 52°C$				
A, C	[0.72; 0.69; 0.02]	15.07×4.70	Compound twinned	14.00×4.85
B, D	[−0.70; 0.72; 0.01]	15.07×4.56	Compound twinned	14.00×4.79

In the rest of the text, we will call this line of coexistence the *crossing line*. We will also use the following terminology for the twinned regions: if the twinned-to-single variant boundaries is parallel (or nearly parallel) to the lamina inside, the region will be called the *X*-region (as it appears twice in the *X*-interface), if not, the region will be called the λ-region. So the *X*-interface consists of two *X*-regions, and the λ-interface of either one λ-region and one *X*-region or of two λ-regions.

3. Experimental observations

3.1. *Used specimens*

A spontaneous formation of *X* and λ-interfaces was observed in two specimens of a Cu–Al–Ni SMA. The specimens were prismatic bars of single crystals, rectangular in austenite. In Table 1, the dimensions and crystallographic orientations of these specimens are listed, for capitals A-B-C-D denoting perpendicularly the faces of each bar. For the experiments, the specimens were electrolytically polished, and the surfaces between each two runs of the experiment were cleaned by ethyl alcohol.

'Specimen #1' was a $12 \times 3 \times 3$ mm bar (in austenite) with orientation close to the principal axes of austenite. By applying an uniaxial compression in direction of the specimen's length, the Specimen #1 can be transformed into a 11 mm long parallelepiped of a single variant of mechanically stabilized 2H martensite (namely, for the orientation of austenite given in Table 1, the obtained variant is variant no. 6 in notation introduced by Sedlák et al. in [16]).

'Specimen #2' was a $15 \times 5 \times 5$ mm bar (in austenite) with axial orientation close to [0 0 1] and the face normals close to [1 1 0] and [−1 1 0] in austenite. By applying an uniaxial compression in direction of the specimen's length, the Specimen #2 can be transformed into a 14 mm long parallelepiped of a Compound twinned structure of martensite (<5% of variant no. 5 in variant no. 6, using the notation of [16] again). Compared to Specimen #1, Specimen #2 had higher transition temperatures (adjusted by annealing the specimen at 250°C for 30 min). It was impossible to remove all twins from this specimen by applying the uniaxial compression in the direction of the specimen length. The reason for this should be sought in the fact that Specimen #2 was cut nearly exactly along the (1 1 0), (1 −1 0) and (0 0 1) planes. Due to such high symmetry of this specimen, the austenite under the compression splits into two different variants of martensite instead of preferring only one of them.

3.2. *Experiment methodology*

Both specimens were subjected to the same experimental procedure:

(1) Specimen was transformed into mechanically stabilized martensite by applying uniaxial compression. The compression was provided in a conventional bench vise. When the specimen seemed to be fully transformed into martensite, it was removed from the vise, but stayed in the martensitic state due to the mechanical stabilization, as outlined in Figure 1(c). No loading maintained during the rest of the experiment. The applied stress was not measured during the stabilizing process. However, as the material is the same, we can expect the critical values to be comparable to these presented in [16].
(2) A small nucleus was induced in the chosen corner of the specimen by a gas lighter. This austenitic nucleus was always surrounded by a complicated system of twinned regions ensuring the compatibility of the nucleus with the mechanically stabilized martensite (Figure 3).
(3) The specimen with a nucleus was heated until it transformed back to austenite. At the start of the transition, the microstructure surrounding the nucleus always simplified into a X or λ-interface. Two different methods of heating were used with the same results (the same interfacial microstructure formed and propagated):
    (a) The specimen was placed in a thermal gradient, i.e. it was heated at the end with the nucleus and cooled at another. The gradient was slowly steepened until the interfacial structure formed and started propagating through the specimen. (For technical detail of the used device and the critical temperatures for propagation, see [4].)
    (b) The whole specimen was immersed in a warm (temperature ranging between 50 and 65°C) water bath.

When the heating of the specimen was interrupted by removing the specimen from the thermal gradient or from the water bath, the propagating boundary stopped in the middle of the specimen, and remained stable until the heating was provided again.

The formed microstructures were observed by an OLYMPUS SZ60 stereomicroscope, and recorded by a uEye UI-2250-C camera (chip size 1/1.8″) with full 1600×1200 pts resolution and acquisition frequency 24 frames per second. The obtained micrographs were converted into a 16-bit grayscale with proper intensity rescaling such that the microstructures were clearly visible.

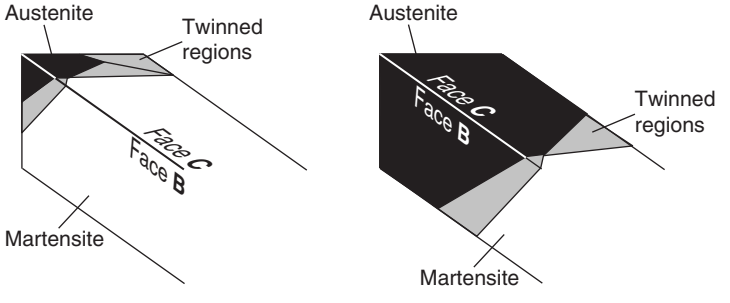

Figure 3. Initial morphology of the nucleus (on the left) and morphology formed after immersing the whole specimen into a warm water bath for approximatively 2 s.

In Figure 3, the evolution of the microstructure from a corner-like nucleus into a fully formed λ-interface in Specimen #1 is outlined.

3.3. *Observed microstructures*

Repeatedly, two different types of interfacial microstructure formed in the examined specimens. It was a λ-interface in Specimen #1 and an *X*-interface in Specimen #2. The morphology of these two interfacial microstructures is outlined in Figure 4. Detailed optical micrographs of the faces with crossing habit planes are in Figure 5. The twinning systems in these microstructures were identified from relative angles between the habit planes and the twinning planes, using the theoretical values found in [10].

The λ-interface in Specimen #1 consisted of two different twinned regions connecting the austenite with single variant of martensite. First of them, spanning over faces C, D and A, was identified as Type-II twins. One of the variants involved in this twinned region was the same as the single variant. Therefore, this system was able to connect compatibly to the single variant over a twinning plane, i.e. the Type-II region was an *X*-region. The second twinned region (a λ-region spanning over faces A, B and C) was identified as Type-I twins.

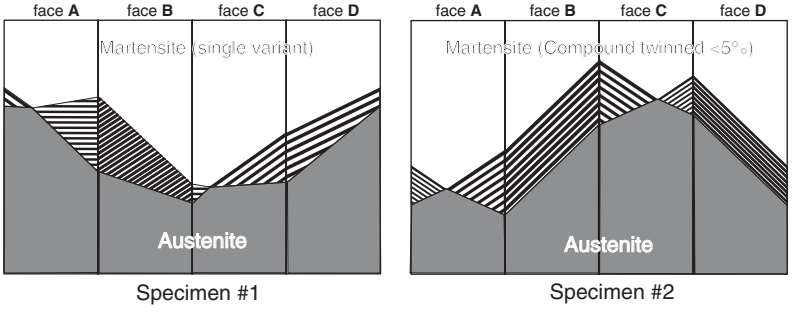

Figure 4. Schematic sketch of the interfacial microstructures observed between austenite and mechanically stabilized martensite during the shape recovery process.
Note: The stripes inside the twinned regions (between austenite and stabilized martensite) show the orientation of twinning planes.

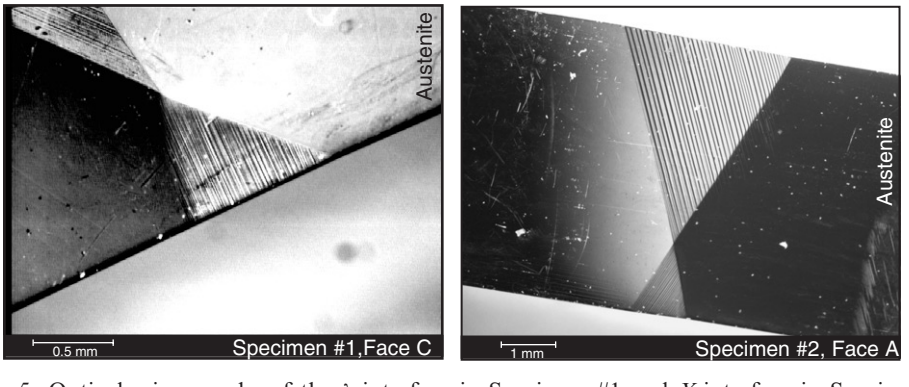

Figure 5. Optical micrographs of the λ-interface in Specimen #1 and *X*-interface in Specimen #2 observed during the shape recovery process.

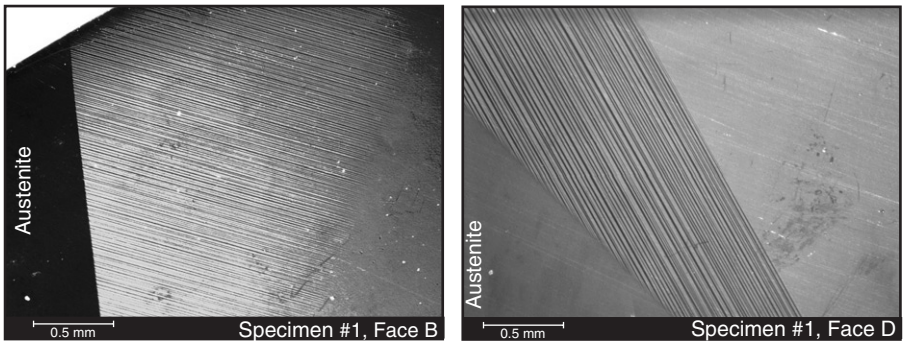

Figure 6. Comparison of two parts of the λ-interface in Specimen #1 (Optical microscopy).
Notes: The Type-I twins (λ-region, on the left) border to the single variant over a fuzzy interface, whereas the Type II (*X*-region, on the right) over one single twinning plane.

The connection of this region to single variant of martensite was provided by a planar, but strongly diffused interface, which had a form of parallel thin needles disappearing in the single variant of martensite (see Figure 6 for comparison of the Type-I and Type-II regions in the λ-interface). The microstructure in Type-I region was also much finer compared to the Type-II region, i.e. the laminates in the Type-I region had considerably lower thickness.

The *X*-interface in Specimen #2 consisted of two similar Type-II regions, one of them spanning over faces A, B and C, the second over C, D and A. Moreover, there regions were also weakly Compound twinned in form of few thin Compound needles penetrating the structure from the mechanically stabilized martensite and disappearing near the habit plane, as will be discussed in more detail and illustrated by optical micrographs in the last paragraph of this section. The positions of the crossing line between faces A and C was not fixed; sometimes the structure was nearly symmetric (the crossings were close to the centres of these faces), in some other cases, one of the region was significantly smaller than the other. Due to the special orientation of the specimen, the intersection of the twinning planes and the habit plane with faces B and D were close to parallel, so the interface at these faces appeared in form of diagonal stripes (Figure 7). The thickness of these stripes was decreasing rapidly near the habit plane, which was a natural consequence of branching of martensitic plates near the transition front. The twins in both regions of the *X*-interface were significantly thicker than in Specimen #1.

One of the possible explanations for the consistent difference between the interfacial microstructures forming in Specimen #1 and Specimen #2 can be that corners at which the austenite nucleates have different crystallographic orientations in these specimens, and thus enable, different geometry of the nuclei. Then, the whole interfacial microstructure can inherit some of the properties of the nucleus.

These microstructures appeared in cca 90% of runs of the experiment. In few cases, different, usually more complicated interfaces, formed and propagated, but always with the concept of two intersecting habit planes preserved. These irregularities can be ascribed to the irreproducibility of the shape of the nucleus or to incomplete previous stress-induced transition into mechanically stabilized martensite. Examples of such rarely observed structures are shown in Figure 8.

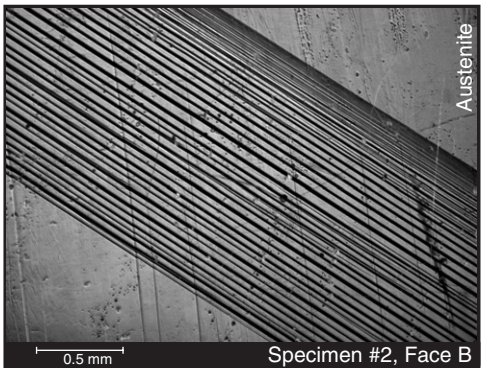

Figure 7. Twinned region observed at faces B and D of Specimen #2 (Optical microscopy).
Notes: Intersection of the specimen's face with the twinning planes and with the habit plane are nearly parallel. The thickness of layers rapidly decreases near the habit plane. Few Compound twins intersecting the whole twinned region are visible.

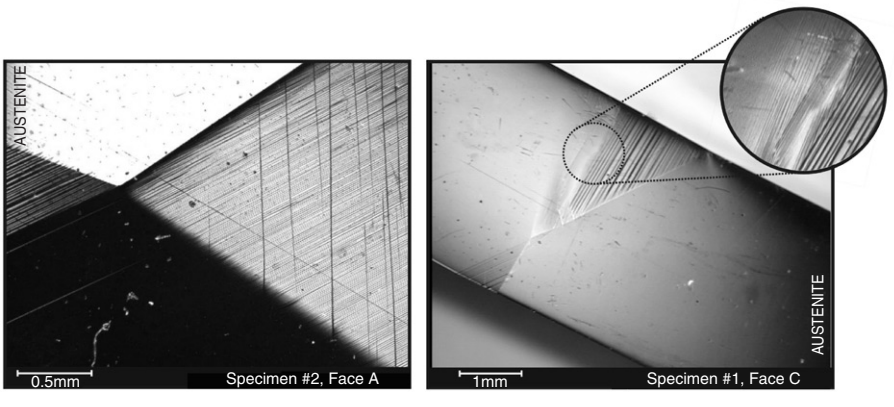

Figure 8. Rarely observed interfacial microstructures (Optical microscopy).
Note: On the left: A λ-interface in Specimen #2, with the λ-region intersected by few Compound twins. On the right: Distorted λ-interface in Specimen #1, with a diffused 'cloud' of extremely fine twins above the λ-region shown in a zoomed area.

3.4. *Observed growth mechanisms*

During the propagation, the micromechanisms of growth of above described interfacial microstructures were observed. The main mechanisms are outlined in Figure 9. (This figure shows a general character of the growth mechanisms only. In our particular case of Specimen #1, 'variant A' corresponds in Figure 9(a, b) to no. 2, 'variant B' to no. 6 and 'variant C' to no. 5, following the notation of [16]. For Specimen #2, it must be taken into account that the denotations 'variant A', 'variant B', and 'variant C' in Figure 9(c) correspond to finely twinned Compound structures).

The λ-region bordering to the mechanically stabilized martensite over a diffused interface was moving by a simultaneous growth of all parallel needles in the

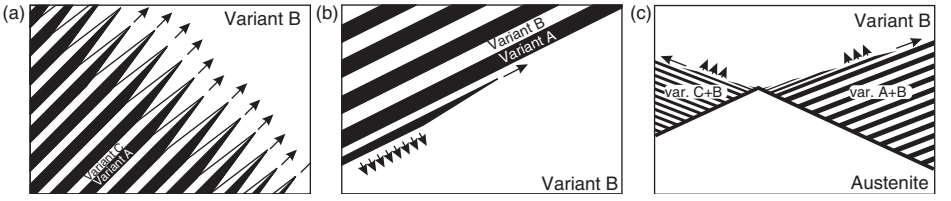

Figure 9. Growth mechanisms observed on the interfacial structures. (a) An epitaxial growth of a λ-region, (b) An *X*-region growing by individual needle's growth and thickening, (c) Nucleation of new needles near the crossing line for the *X*-interface.

microstructure, whereas the *X*-regions (both in the λ and *X*-interface) were propagating by growth of individual needles along the interface and by thickening of such needles. Sometimes, two or three thin needles also merged into a thicker one during the growth. Nucleation of new martensitic needles was observed at face A of Specimen #2 in the region near the crossing line, as shown in Figure 9(c). The propagation of the whole *X*-microstructure was thus, driven by local circumstances around the crossing line. In the λ-interface, the nucleation mechanism was not so clear. The Type-II needles of the *X*-region nucleated at the crossing line at face A again, whereas thin Type-I needles of the λ-region seemed to appear spontaneously at the edge between faces A and B.

There were strong differences in velocities of growth of individual needles. Especially, the very thin needles grew slowly and continuously (few millimeters per second), whereas thick needles appeared abruptly, at velocities uncapturable by the acquisition frequency of the used camera. This is fully consistent with the jerky character of the motion of the interface mentioned in the Introduction.

3.5. *Weakly non-classical boundaries*

As mentioned in Section 3.1, the mechanically stabilized martensite in Specimen #2 contained less than 5% of another variant in a form of Compound twins. The Compound structure remained also in the *X*-regions of the interfacial microstructure.

Let us now construct such microstructure created by crossing of the Type-II and Compound systems. To do that, we will shortly recapitulate a part of more general theoretical investigation of Cu–Al–Ni martensitic structures by Chu and James [17], who have proved that the Compound twins can cross compatibly with both the Type-I and Type-II systems. Let A and B be two martensitic variants able to form Type-II twins, and A' and B' be their Compound counterparts, i.e. variants able to form Compound twins with them. Then, the variants A' and B' can also form a Type-II structure, and we can write following four compatibility conditions (4) for Type-II twinning planes $\boldsymbol{n}_{AB}$ and $\boldsymbol{n}_{A'B'}$ and Compound twinning planes $\boldsymbol{n}_{AA'}$ and $\boldsymbol{n}_{BB'}$:

$$\mathbf{U}_A - \mathbf{R}_{AB}\mathbf{U}_B = \boldsymbol{b}_{AB} \otimes \boldsymbol{n}_{AB}, \tag{6}$$

$$\mathbf{U}_{A'} - \mathbf{R}_{A'B'}\mathbf{U}_{B'} = \boldsymbol{b}_{A'B'} \otimes \boldsymbol{n}_{A'B'}, \tag{7}$$

$$\mathbf{U}_A - \mathbf{R}_{AA'}\mathbf{U}_{A'} = \boldsymbol{b}_{AA'} \otimes \boldsymbol{n}_{AA'}, \tag{8}$$

$$\mathbf{U}_B - \mathbf{R}_{BB'}\mathbf{U}_{B'} = \boldsymbol{b}_{BB'} \otimes \boldsymbol{n}_{BB'}, \tag{9}$$

Table 2. Comparison of habit plane normals $\boldsymbol{n}$, shearing vectors $\boldsymbol{a}$ and admissible volume fractions λ for a classical austenite-to-Type-II boundary and for a non-classical boundary between austenite and the microstructure (14) with $\Lambda = 0.95$.

	Type-II Variants no. 3 and no. 6	Type-II with 5% of Compound counterparts	Difference
$\boldsymbol{n}$	(−0.6240; −0.7371; 0.2595)	(−0.6339; −0.7353; 0.2399)	1.15°
$\boldsymbol{a}$	[0.0721; −0.0617; −0.0144]	[0.0710; −0.0608; −0.0121]	1.25°
λ	0.3008	0.3068	2.0%

where $\mathbf{R}_{IJ}$ are the mutual rotations between variants I and J, and $\boldsymbol{b}_{IJ}$ are the shearing vectors for particular twinning systems. In a compatible structure, the mutual rotation between A and B' can be written as superposition of rotations $\mathbf{R}_{AB}$ and $\mathbf{R}_{BB'}$ or equivalently, of rotations $\mathbf{R}_{AA'}$ and $\mathbf{R}_{A'B'}$, which gives

$$\mathbf{R}_{AB}\mathbf{R}_{BB'} = \mathbf{R}_{AA'}\mathbf{R}_{A'B'}. \tag{10}$$

If the pair-wise compatibility Equations (6)–(9) are satisfied, this condition on rotation matrices $\mathbf{R}_{IJ}$ is a sufficient condition for compatibility of the whole microstructure [10]. Indeed, in our case of a cubic-to-orthorhombic transition, where the Compound twinning planes can be chosen such that

$$\boldsymbol{n}_{AA'} = \boldsymbol{n}_{BB'}, \tag{11}$$

it is easy to prove that the Type-II twinned structures

$$\mathbf{M}_{AB} = (1-\lambda)\mathbf{U}_A + \lambda\mathbf{R}_{AB}\mathbf{U}_B \tag{12}$$

$$\text{and } \mathbf{M}_{A'B'} = (1-\lambda)\mathbf{U}_{A'} + \lambda\mathbf{R}_{A'B'}\mathbf{U}_{B'}, \tag{13}$$

can border compatibly over a Compound twinning plane $\boldsymbol{n}_{AA'}$ as long as the volume fractions λ are the same in $\mathbf{M}_{AB}$ and $\mathbf{M}_{A'B'}$.

Now, we are able to construct the deformation gradient of our microstructure from quasiconvexification (2) by stating

$$\mathbf{M} = \Lambda\mathbf{M}_{AB} + (1-\Lambda)\mathbf{R}_{AA'}\mathbf{M}_{A'B'}, \tag{14}$$

where Λ is a volume fraction of variants A and B in their Compound counterparts. In our case of $\Lambda > 0.95$, the presence of variants A' and B' does not have any measurable geometric effect on the macroscopic morphology of the interface. In Table 2, the results of numeric analysis of such interface are listed. For $\Lambda = 0.95$, the volume fraction λ (i.e. the volume fraction of variant A in variant B and of variant A' in variant B') was numerically determined such that

$$\det(\mathbf{M}^T\mathbf{M} - \mathbf{I}) = 0, \tag{15}$$

which is a compatibility condition equivalent to (1) [18]. For such λ, the habit plane orientation and the shearing vector were determined, following the algebraic procedure developed by James and Ball [9]. As it can be seen from Table 2, the difference in the habit plane orientations (1.25°) is comparable to the level of expectable experimental errors. Similarly, the difference in the volume fraction is too small to be proved

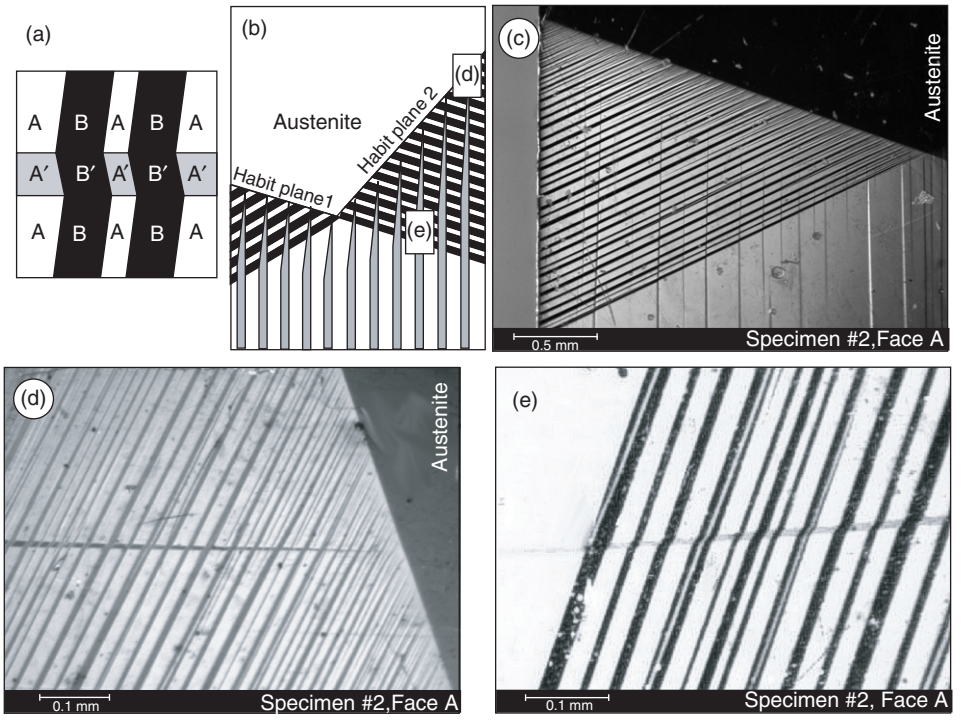

Figure 10. Weakly non-classical boundaries: (a) Microstructure of crossing Compound (A–A' and B–B') and Type-II (A–B and A'–B') twinning systems, (b) Schematic sketch of a global morphology (white rectangles correspond to the detailed optical micrographs (d) and (e)), (c) Optical micrograph of a weakly non-classical boundary in Specimen #2, (d) A zoomed area of one Compound needle disappearing in the vicinity of the habit plane, (e) Another Compound needle entering the Type-II twinned region – the kinks on the Type-II twins are clearly visible.

by any measurements. In the other words, the only evidence we have that the interfaces observed in Specimen #2 are not classical is the presence of visible Compound needles in optical micrographs.

For this reason, we decided to call such interface between **M** and austenite the 'weakly non-classical boundary'. Anyway, to the author's best knowledge, no such interfaces have been documented in the available literature yet. At the microlevel, the microstructure looks like as it is outlined in Figure 10(a): The crossing with Compound needles induces kinks on layers of variants A and B (see also Figure 10(e) for a detailed optical micrograph of these kinks). Mesoscopically, the Compound needles penetrate the Type-II regions and end as very thin in the vicinity of the habit plane (Figure 10(b–d)).

4. Summary

Spontaneous formation of X and λ-interfaces in single crystals of the Cu–Al–Ni was observed. Both in the thermal gradient and in homogeneous heating (after nucleation provided by localized heating), these interfacial microstructures formed and propagated through the specimen. The motion of the microstructures was enabled by nucleation and growth of new needles, appearing either near the intersection of the habit planes or at the

edge of the specimen. Weakly non-classical boundaries (planar interfaces between austenite and higher-order laminate of martensite) were observed during the shape recovery process of a Compound twinned specimen.

Acknowledgements

This work was supported by project AV0Z 20760514 of the Institute of Thermomechanics ASCR. Authors would like to acknowledge J. Kopeček, V. Novák and S. Ignácová (Institute of Physics ASCR) for specimen preparation and DSC measurements. The first author would also like express his gratitude to Prof. Sir J. M. Ball (Oxford University) for support, comments and discussions.

Notes

1. Bhattacharya [10] mentions only two alloys able to form an austenite–to–single variant habit plane. For the overwhelming majority of known SMAs, the habit plane is possible only between austenite and a microstructured martensite.
2. This effect does not involve any reordering or lattice distortion as it is in the case of *thermal stabilization* induced by ageing in martensite.

References

[1] K.F. Hane, *Microstructures in thermoelastic martensites*, Ph.D. thesis, University of Minnesota, 1998.
[2] Z.S. Basinski and J.W. Christian, Acta Metall. 2 (1954), pp. 148–166.
[3] R.J. Salzbrenner and M. Cohen, Acta Metall. 27 (1979), pp. 739–748.
[4] H. Seiner, M. Landa, and P. Sedlák, Proc. of the Estonian Acad. of Scien. 56 (2007), pp. 218–225.
[5] S. Ignácová, T. Černoch, V. Novák et al., Poster presented at ESOMAT 2006, Bochum, Germany, 2006.
[6] H. Sakamoto and K. Shimizu, Trans. of the Japan Inst. of Metals 25 (1984), pp. 845–854.
[7] T.W. Shield, J. Mech. Phys. Solids 43 (1995), pp. 869–895.
[8] G. Ruddock, Arch. Rat. Mech. Anal. 127 (1994), pp. 1–39.
[9] J.M. Ball and R.D. James, Arch. Rat. Mech. Anal. 100 (1987), pp. 13–52.
[10] K. Bhattacharya, *Microstructure of Martensite*, Oxford University Press, Oxford, 2003.
[11] X. Balandraud and G. Zanzotto, J. Mech. Phys. Solids 55 (2007), pp. 194–224.
[12] J.M. Ball and C. Carstensen, J. de Phys. IV 7 (1997), pp. 35–40.
[13] G. Dolzmann, *Variational Methods for Crystalline Microstructure-Analysis and Computation*, Springer Verlag, Berlin, 2003.
[14] P. Picornell, V.A. L'vov, J. Pons et al., Mat. Sci. Eng. A. 438–440 (2006), pp. 755–762.
[15] L.C. Brinson, J. of Intell. Mater. Syst. and Struct. 4 (1993), pp. 229–242.
[16] P. Sedlák, H. Seiner, M. Landa et al., Acta Mat. 53 (2005), pp. 3643–3661.
[17] C. Chu and R.D. James, J. de Phys IV 5 (1995), pp. 143–149.
[18] J.M. Ball, Mat. Sci. Eng. A. 378 (2004), pp. 61–69.